San Jose State University

SJSU ScholarWorks

Faculty Research, Scholarly, and Creative Activity

1-1-2023

Investigation to Density and Metallurgical Characteristics of Selective Laser Melted Ti-5Al-5 V-5Mo-3Cr Versus Ti-6Al-4 V

David Yan
San Jose State University, david.yan@sjsu.edu

Roman Bolzowski
San Jose State University, roman.bolzowski@sjsu.edu

Follow this and additional works at: https://scholarworks.sjsu.edu/faculty_rsca

Investigation to Density and Metallurgical Characteristics of Selective Laser Melted Ti-5Al-5V-5Mo-3Cr Vs. Ti-6Al-4V

David Yan[1]* and Roman Bolzowski[1]

[1]Department of Aviation and Technology, San José State University, One Washington Sq, San Jose, CA 95192

*Corresponding author: E-mail: david.yan@sjsu.edu Tel.: 408-924-3222

Abstract: Ti-5Al-5V-5Mo-3Cr (Ti-5553) is a metastable near beta titanium alloy with excellent fatigue performance and corrosion resistance. Hence, it is of significant importance in several high-performance aerospace applications such as aircraft landing gear components. The selective laser melting (SLM) technique shows great potential compared to subtractive methods in generating complex geometries. However, the poor surface finish of the SLMed Ti-5553 components means that post-machining is required to achieve the desired surface quality and dimensional accuracy. Although there is a profound knowledge about the surface integrity of SLMed α + β Ti alloys (typically Ti-6Al-4V), there is a lack of understanding regarding the microstructure of internal subsurface layers of SLMed Ti-5553 components. In this paper, experimental studies were performed on SLM of Ti-5553 and Ti-64 to determine the effect of SLM parameters on the surface integrity of SLMed Ti components. The density and subsurface microstructure of printed Ti components were measured and evaluated in relation to the SLM conditions.

1. Introduction

Titanium (Ti) alloys have been increasingly used in the aerospace, biomedical, and chemical engineering industries, owing to their desirable mechanical properties, including high strength-to-density ratio, outstanding fatigue life, good corrosion resistance, etc. [1-4]. Of particular interest is that the β Ti alloys (e.g., Ti-5553) have been critically chosen for structural components applications in the aerospace industry, mostly due to their excellent performance-to-density ratio and ultimate tensile strength of up to 1300 MPa [5-7]. Currently, the production of parts made of wrought Ti-5553 includes a complex sequence of different thermo-mechanical and post-surface machining steps to gain the desired microstructure and surface quality [8, 9]. However, in general, machining Ti-5553 parts using conventional techniques is challenging, since the short tool life and low cutting speed give rise to long processing times and high machining costs [10]. To overcome the problems of machining and incorporate the appropriate thermal-mechanical conditions for customized Ti-5553 part production with tailored geometry and properties, additive manufacturing (AM) methods can be considered an effective solution.

AM has gained great attention among researchers and manufacturing industries due to its advantageous capabilities such as freedom of design, on-demand manufacturing, reduced raw material wastage, and low energy consumption [11]. In the last decade, various AM techniques for processing metallic materials were developed. Some of these techniques utilize wire as initial material (e.g., shaped metal deposition) and others use metallic powders (e.g., selective laser sintering (SLS), selective laser melting (SLM), and electron beam melting (EBM)) [12]. Each of these technologies has its advantages and disadvantages. SLM is characterized by medium productivity and good repeatability and thus, it is considered a suitable method for direct manufacturing of high-quality parts with low to medium quantity [13]. SLM is a layer-by-layer technique that is composed of a powder bed on a build plate and a moving laser heat source that

melts the powder and moves along scan tracks [14]. Specifically, with the data set of a sliced digital model imported from the relevant 3D CAD model, the laser scans and selectively melts a portion of the initial powder bed. Then the build plate moves downwards by a predetermined layer thickness value, followed by respreading a new layer of powder on top of the previous layer. And then the new powder layer is scanned and melted by the laser again, along with some of the former layers, to facilitate a bond or connection between the two subsequent layers. This process repeats multiple times based on the preset height of the part along the building direction for numerous layers until the entire part is fabricated [15]. There are more than a dozen of SLM parameters that can be varied and fine-tuned to result in a SLMed part with the desired physical, mechanical, and microstructure properties. Indeed, the laser power (P), laser scanning speed (v), hatch spacing (h), and layer thickness (t) are the four most common adjustments used to optimize the SLM process to achieve the ideal part quality and production efficiency [16, 17].

So far, most of the research on the SLM of titanium alloys and resultant properties has been focused on Ti-6Al-4V (i.e., Ti-64), and an extensive and critical review of SLM of Ti-64 in terms of SLM parameters, defects, and various post-processing techniques has been notably presented [17]. Regarding the SLM of Ti-5553, Schwab et al. [16, 18] investigated the effect of SLM parameters on the density, microstructure, and mechanical properties of SLMed Ti-5553 components. They reported that bulk samples with a relative density of 99.95% and a two-phase, i.e., α and β phase microstructure were successfully built. They also concluded that the SLM offers new and promising perspectives for industrial applications of Ti-5553.

Indeed, the SLM technique shows great potential compared to the conventional machining techniques in processing Ti-5553, and to the best knowledge of the authors, the publicly accessible literature on the SLM of Ti-5553 is limited. Therefore, in this present research, preliminary experimental studies were conducted on SLMed Ti-5553 and Ti-64. The effect of SLM parameters on the density and microstructure of the printed Ti-5553 and Ti-64 components were assessed and compared through optical microscopy (OM) and scanning electron microscopy (SEM) characterizations.

2. Experimental Procedure

An EOS M 100 machine equipped with a 200 W (theoretical power) YB-fiber laser was employed to print all Ti-5553 and Ti-64 samples. The spot size of the laser beam was about 40 μm in diameter at the focal point. High-purity argon (purity 99.999%) acted as protective gas during the entire printing process. The substrate plate is made of commercial pure titanium.

The powders used in this research were a plasma-atomized Ti-5553 powder provided by AP&C (A GE Additive Company) with a size of 20 to 63 μm, a density of 4.65 g/cm^3 [19, 20], and the chemical compositions (wt.%) of 5.07Al-4.86V-4.85Mo-2.93Cr-0.37Fe-0.08O-0.03N and (Bal) Ti. While Ti-64 powder was supplied by EOS (manufacturer of EOS M 100) with a size of 39 ±3 μm, a density of 4.4 g/cm^3, and chemical compositions (wt.%) of 5.50-6.75Al-3.50-4.50V-0.30Fe-0.20O-0.05N-0.08C-0.01H and (Bal.) Ti.

It is essential to optimize the heat input to develop a better print recipe for a new material such as Ti-5553. To relate the four most influencing parameters, as detailed in the Introduction section, an energy density function, i.e., volumetric energy density (VED) has been developed. In which the VED function relates to the laser power (P), scan speed (v), hatch spacing (h), and layer thickness (t) as hereby represented by equation (1) with stated units.

$$VED \ (J/mm^3) = \frac{P \ (W)}{v \ (mm/s)*h(\mu m)*t(\mu m)} \tag{1}$$

To the best knowledge of the authors, for the first time EOS M 100, with a very small laser spot size of 40 μm (typically 80μm), was used to print Ti-5553 components. Thus, the EOS' default printing parameters for Ti-64 were adopted and employed in the printing of Ti-5553 and Ti-64 samples. And the go-to exposure strategy recommended by the EOS company was also utilized, in which a striping scheme with 5mm stripe width (i.e., length of each vector line) and 0.1mm overlap as a scanning strategy was deployed in all sample printing in this preliminary study. Table 1 lists the printing parameters while Figure 1 presents the stripe pattern as a scanning strategy for the printing process.

Table 1 The SLM parameters used in the present research

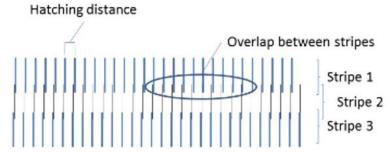| VED (J/mm^3)	Laser power (W)	Scanning speed (mm/s)	Layer thickness (μm)	Hatch spacing (μm)
62.5	90	1200	30	40

Figure 1 Illustration of stripe pattern with 5mm stripe width (i.e., length of each vector line) and 0.1mm overlap as scanning strategy used for printing all Ti-5553 and Ti-64 samples.

To investigate the effect of SLM parameters on the density and microstructure of the printed Ti-5553 and Ti-64 components, five (5) rectangular prism Ti-5553 samples, with a width, length, and height of 24mm, 32mm, and 30mm, and five (5) cylindrical Ti-64 samples, with a diameter of 6 mm and a height of 30mm, respectively, were printed.
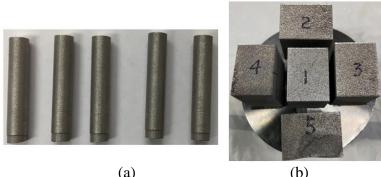
After printing the Ti-5553 and Ti-64 samples, the density of the printed Ti samples was calculated by dividing the mass of the sample by its volume. A CGOLDENWALL electronic balance with a resolution of 0.01g and an electronic caliper (resolution of 0.1mm) was used to measure the mass and dimensions of the printed samples. The volume of the sample was directly calculated by substituting the measured sample dimensions into the volume equations for the rectangular prism and cylindrical shape for the Ti-5553 and Ti-64 samples, respectively.

To study the samples' subsurface microstructure associated with the printing parameters and scanning strategy, the printed Ti-5553 and Ti-64 samples were sectioned in the transverse and longitudinal direction (i.e., the building direction-z axis). All cross-section samples were mounted, ground, and polished with standard metallographic practice, i.e., SiC #320 to 600 sandpapers for grinding and MicroPolish 6 μm and 0.3 μm Alumina-water slurry for final polishing. Then the polished samples were etched using Kroll's etchant (2ml HF and 6ml HNO_3 in 100ml H_2O) for 20s. Subsequently, the etched samples were examined via Nikon TE-300 optical microscope (OM) and FEI Quanta 200 environmental scanning electron microscope (SEM) with an EBSD detector.

3. Results and discussion

3.1 Density measurement and relative density comparison

Figure 2 (a) and (b) show images of Ti-64 and Ti-5553 samples printed using an EOS M 100 machine at the laser power of 100 W, a scan speed of 1400 mm/s, a layer thickness of 30 μm and a hatch spacing of 40 μm. And the scanning strategy of a stripe scheme with 5mm stripe width and 0.1mm overlap was deployed during the printing. Observations of these two groups of printed samples show that surface-defect-free prints were achieved under the current SLM conditions and scanning strategy. It can also be seen from the figure that both printed Ti-64 and Ti-5553 samples had an oxidized surface due to the high heat input applied.

| (a) | (b) |

Figure 2 Photos of two groups of Ti samples printed using an EOS M 100 machine at the laser power of 100 W, the scan speed of 1400 mm/s, the layer thickness of 30 μm, and hatch spacing of 40 μm and deploying the stripe scheme as scanning strategy with 5mm stripe width and 0.1mm overlap, (a) cylindrical Ti-64 samples, with a diameter of 6 mm and a height of 30mm, and (b) rectangular prism Ti-5553 samples, with a width, length and height of 24mm, 32mm and 30mm, respectively.

To determine the average density for printed Ti-64 and Ti-5553 samples, the mass of five (5) Ti-64 and Ti-5553 samples were individually weighted by the electronic balance (resolution of 0.01g), and the dimensions of these samples were also measured individually using an electronic caliper (resolution of 0.1mm). Table 2 lists the average mass, volume, and density of printed Ti-64 and Ti-5553 samples, manufacturers' virgin powder density, and relative density.

Table 2 The average mass, volume, and density of printed Ti-64 and Ti-5553 samples, manufacturers' virgin powder density, and relative density

Ti sample	Sample mass (g)	Sample volume (cm^3)	Sample density (g/ cm^3)	Manufacturer' density (g/ cm^3)	Relative density %
Ti-64	3.71	0.848	4.376	4.41	99.23
Ti-5553	105.65	23.04	4.586	4.65	98.61

It can be found from Table 2 that the relative densities of printed Ti-64 and Ti-5553 sample are 99.23% and 98.61%, respectively, and the printed Ti-64 sample has a higher relative density than Ti-5553 sample. It was evident that the SLM parameters used in the present research were optimized for Ti-64, thus, leading to a higher relative density than the one of Ti-5553. The poor/low relative density of Ti-5553 may be due to the additional compositions of Mo and Cr compared to Ti-64 that cause a lack of fusion which, in turn, contributes to internal porosity level [15].

Figure 3 (a) and (b) present SEM micrographs of cross sections (i.e., y-z plane, along the building direction-z axis) of printed Ti-64 and Ti-5553 samples. Observation of these two SEM images shows that there were more white particles /dots shown in the cross-section of Ti-5553 than that of Ti-64, which can be related to the pore volume presented in these two Ti samples [16]. Thus, the printed Ti-5553 sample had more pore volume than that of Ti-64 showing a lower relative density (i.e., 98.61%) when compared to Ti-64 (i.e., 99.23%). This result may be caused by a low overlap setting in the stripe scheme as a scanning strategy in the printing of Ti-5553 samples, according to Schwab et al. [16]. Indeed, the observation of the porosity level shown in SEM micrographs of cross sections of Ti-64 and Ti-5553 samples correlated well with the calculated relative densities for Ti-64 and Ti-5553 listed in Table 2.
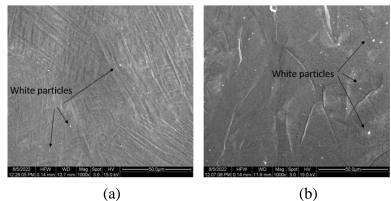

(a)   (b)

Figure 3 SEM micrographs of cross sections (i.e., y-z plane, along the building direction-z axis) of (a) Ti-64 and (b) Ti-5553 samples, printed at the laser power of 100 W, a scan speed of 1400 mm/s, a layer thickness of 30 μm and a hatch spacing of 40 μm, respectively, showing more white particles in Ti-5553 compared to Ti-64, indicating higher porosity level in printed Ti-5553 samples than that of Ti-64.

3.2 Subsurface microstructure characterization

Figure 4 (a) and (b) show higher magnification SEM micrographs of cross sections (i.e., x-y plane, normal to the building direction-z axis) of printed Ti-64 and Ti-5553 samples. Observation of figure 4 (a)-the higher magnification SEM image of the as-built Ti-64 subsurface shows that there were fine columnar prior-β grains filled with α' martensite on the surface. The variations, morphologies, and constituent phases obtained from the present study were similar to the results of Singla et al. [17], in particular, α' martensite was mostly developed during SLM of Ti-64. While by examining figure 4 (b)-the higher magnification SEM image of the as-built Ti-5553 subsurface, it can be seen that the α phase had been precipitated along the continuous array of grain boundaries which was consistent with the findings of Bakhshivash et al. [15].
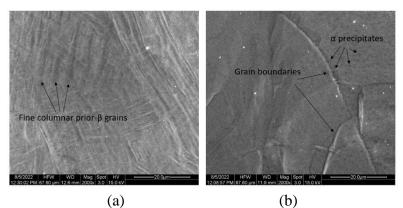
(a)   (b)

Figure 4 Higher SEM micrographs of cross sections (i.e., x-y plane, normal to the building direction-z axis) of (a) printed Ti-64 sample showing fine columnar prior-β grains filled with α' martensite inside the cross-section, and (b) printed Ti-5553 sample presenting grain boundaries with α precipitates appeared in the cross-section.

Figure 5 (a) and (b) show higher magnification SEM micrographs of cross sections (i.e., y-z plane, along the building direction-z axis) of as-built Ti-64 and Ti-5553 samples. Examination of figure 5 (a)-the higher magnification SEM image of the as-built Ti-64 subsurface layer shows that the microstructures were composed of acicular α' phase with minor α +β lamellae randomly organized across the surface. These findings were consistent with the results of Singla et al. [17] since they reported that the acicular or needle-like features were resulted from α' phase precipitations due to the rapid cooling during the SLM process. By observing figure 5 (b)- the higher magnification SEM image of the as-built Ti-5553 subsurface layer, it can be seen that the balling effects occurred during the printing of the Ti-5553 sample. To the best knowledge of the authors, for the first time, the balling effect was recorded during the printing of Ti-5553. And the observed balling effect in the SLMed Ti-5553 was similar to the findings of many researchers [17] who conducted the SLM of Ti-64 experiments and found that the existence of the balling effect was due to the use of the high volumetric energy density (VED) during the SLM process [17].
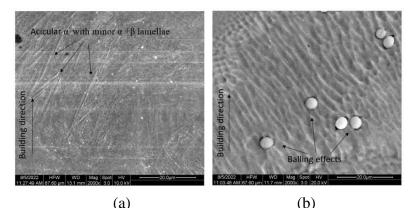

(a)   (b)

Figure 5 Higher SEM micrographs of cross sections (i.e., y-z plane, along the building direction-z axis) of (a) printed Ti-64 sample showing acicular α' phase with minor α +β lamellae randomly organized across the cross-section, and (b) printed Ti-5553 sample presenting the balling effects in the cross-section for the first time.

4. Conclusions

The SLM of Ti-64 and Ti-5553 experiments were successfully performed using the EOS' default printing parameters for Ti-64 under the go-to exposure strategy. The actual densities of as-built Ti-64 and Ti-5553 samples were determined relating to their relative densities. The microstructures of printed Ti-64 and Ti-5553 samples were characterized via optical microscopy (OM) and scanning electron microscopy (SEM). Based on the results obtained from this present study, the following conclusions can be drawn:

1. Ti-5553 was successfully printed by EOS M 100 with a small laser spot size for the first time achieving a sufficient relative density of 98.61 % compared to that of 99.23 for Ti-64.

2. For the first time the balling effect was recorded during SLM of Ti-5553.

3. Microstructures of as-built Ti-5553 include an α phase that was precipitated along the continuous array of grain boundaries.

References
1. Kaynak Y, Gharibi A, Yılmaz U, Köklü U, Aslantaş K (2018) A comparison of flood cooling, minimum quantity lubrication and high pressure coolant on machining and surface integrity of titanium Ti-5553 alloy. Journal of Manufacturing Processes 34:503-512. doi:https://doi.org/10.1016/j.jmapro.2018.06.003

2. Zheng Y, Williams REA, Fraser HL (2016) Characterization of a previously unidentified ordered orthorhombic metastable phase in Ti-5Al-5Mo-5V-3Cr. Scripta Materialia 113:202-205. doi:http://dx.doi.org/10.1016/j.scriptamat.2015.10.037

3. Barriobero-Vila P, Requena G, Schwarz S, Warchomicka F, Buslaps T (2015) Influence of phase transformation kinetics on the formation of α in a β-quenched Ti–5Al–5Mo–5V–3Cr–1Zr alloy. Acta Materialia 95:90-101. doi:10.1016/j.actamat.2015.05.008

4. Boyne A, Wang D, Shi RP, Zheng Y, Behera A, Nag S, Tiley JS, Fraser HL, Banerjee R, Wang Y (2014) Pseudospinodal mechanism for fine α/β microstructures in β-Ti alloys. Acta Materialia 64:188-197. doi:10.1016/j.actamat.2013.10.026

5. Boyer RR (1996) An overview on the use of titanium in the aerospace industry. Materials Science and Engineering: A 213 (1-2):103-114

6. Ahmed M, Li T, Casillas G, Cairney JM, Wexler D, Pereloma EV (2015) The evolution of microstructure and mechanical properties of Ti–5Al–5Mo–5V–2Cr–1Fe during ageing. Journal of Alloys and Compounds 629:260-273. doi:10.1016/j.jallcom.2015.01.005

7. Ghosh A, Sivaprasad S, Bhattacharjee A, Kar SK (2013) Microstructure–fracture toughness correlation in an aircraft structural component alloy Ti–5Al–5V–5Mo–3Cr. Materials Science and Engineering: A 568:61-67. doi:10.1016/j.msea.2013.01.017

8. Stewart Veeck, D.L., Boyer, R., Briggs, R., (2004) The castability of Ti-5553 alloy, Adv. Mater. Process. 162

9. Dehghan-Manshadi, A., Dippenaar, R.J., (2011) Development of α-phase morphologies during low temperature isothermal heat treatment of a Ti–5Al–5Mo–5V–3Cr alloy, Mater. Sci. Eng. A 528, 1833–1839

10. Baili, M.,Wagner,V., Dessein, G., Sallaberry, J., Lallement, D., (2011) An experimental investigation of hot machining with induction to improve Ti-5553 machinability. Appl Mech Mater, 62:67–76

11. Huang, S. H., Liu, P., Mokasdar, A., Hou, L., (2013) Additive manufacturing and its societal impact: a literature review, International Journal of Advanced Manufacturing Technology, 67: 5-8, 1191–1203

12. Frazier, W. E., (2014) Metal additive manufacturing: a review," Journal of Materials Engineering and Performance, vol. 23, no. 6, pp. 1917–1928

13. Levy, G. N., Schindel, R., Kruth, J. P., (2003) Rapid manufacturing and rapid tooling with layer manufacturing (LM) technologies, state of the art and future perspectives," CIRP Annals—Manufacturing Technology, vol. 52, no. 2, pp. 589–609

14. L. Löber, F.P. Schimansky, U. Kühn, F. Pyczak, J. Eckert, Selective laser melting of a beta-solidifying TNM-B1 titanium aluminide alloy, J. Mater. Process. Technol. 214 (2014) 1852–1860.

15. Bakhshivash, S., et al., (2019) Printability and microstructural evolution of Ti-5553 alloy fabricated by modulated laser powder bed fusion. The International Journal of Advanced Manufacturing Technology, 103(9): 4399-4409

16. Schwab, H., et al., (2016) Microstructure and mechanical properties of the near-beta titanium alloy Ti-5553 processed by selective laser melting. Materials & Design, 105: 75-80.

17. Singla, A.K., et al., (2021) Selective laser melting of Ti6Al4V alloy: Process parameters, defects and post-treatments. Journal of Manufacturing Processes, 64: 161-187.

18. Schwab, H., et al., (2017) Processing of Ti-5553 with improved mechanical properties via an in-situ heat treatment combining selective laser melting and substrate plate heating. Materials & Design, 130: p. 83-89.

19. Leyens, C. and M. Peters, (2003) Titanium and titanium alloys: fundamentals and applications. John Wiley & Sons.

20. Zopp, C., et al., (2017) Processing of a metastable titanium alloy (Ti-5553) by selective laser melting. Ain Shams Engineering Journal, 8(3): 475-479.